



This is a repository copy of *Model driven design for integrated twin screw granulator and fluid bed dryer via flowsheet modelling.*

White Rose Research Online URL for this paper:

<https://eprints.whiterose.ac.uk/191280/>

Version: Published Version

Article:

Ge Wang, L., Omar, C. orcid.org/0000-0002-7839-608X, Litster, J. orcid.org/0000-0003-4614-3501 et al. (6 more authors) (2022) Model driven design for integrated twin screw granulator and fluid bed dryer via flowsheet modelling. *International Journal of Pharmaceutics*, 628. 122186. ISSN 0378-5173

<https://doi.org/10.1016/j.ijpharm.2022.122186>

Reuse

This article is distributed under the terms of the Creative Commons Attribution (CC BY) licence. This licence allows you to distribute, remix, tweak, and build upon the work, even commercially, as long as you credit the authors for the original work. More information and the full terms of the licence here:

<https://creativecommons.org/licenses/>

Takedown

If you consider content in White Rose Research Online to be in breach of UK law, please notify us by emailing eprints@whiterose.ac.uk including the URL of the record and the reason for the withdrawal request.



eprints@whiterose.ac.uk
<https://eprints.whiterose.ac.uk/>



Model driven design for integrated twin screw granulator and fluid bed dryer via flowsheet modelling

Li Ge Wang^{a,b}, Chalak Omar^b, James Litster^b, David Slade^a, Jianfeng Li^c, Agba Salman^b, Stefan Bellinghausen^a, Dana Barrasso^a, Niall Mitchell^a

^a Siemens Process Systems Engineering, Hammersmith, London, UK

^b Department of Chemical and Biological Engineering, University of Sheffield, UK

^c Siemens Process Systems Engineering, Parsippany, NJ, USA

ARTICLE INFO

Keywords:

Model Driven Design
Twin Screw Granulator
Fluid Bed Dryer
Continuous Manufacturing
Flowsheet Modelling
Global System Analysis

ABSTRACT

This paper presents a flowsheet modelling of an integrated twin screw granulation (TSG) and fluid bed dryer (FBD) process using a Model Driven Design (MDD) approach. The MDD approach is featured by appropriate process models and efficient model calibration workflow to ensure the product quality. The design space exploration is driven by the physics of the process instead of extensive experimental trials. By means of MDD, the mechanistic-based process kernels are first defined for the TSG and FBD processes. With the awareness of the underlying physics, the complementary experiments are carried out with relevance to the kinetic parameters in the defined models. As a result, the experiments are specifically purposeful for model calibration and validation. The L/S ratio (liquid to solid ratio) and inlet air temperature are selected as the Critical Process Parameters (CPPs) in TSG and FBD for model validation, respectively. Global System Analysis (GSA) is further performed to assess the uncertainty of CPPs imposed on the Critical Quality Attributes (CQAs), which provides significant insights to the exploration of the design space considering both TSG and FBD process parameters.

1. Introduction

Continuous manufacturing (CM) of the formulated products is quickly being adopted in the pharmaceutical industry but also presents a grand challenge in quality control of the formulated products. The novelty of continuous manufacturing for the formulated products lies in the integration of individual unit operations, which has a great deal of potential to facilitate agility, flexibility, and robustness in the pharmaceuticals manufacture (Lee et al., 2015). In view of this, the development and implementation of mathematical modelling of the manufacturing flowsheet has become increasingly appealing to the industry and regulatory authorities (Boukouvala et al., 2012). For example, a dynamic flowsheet model development is presented where sensitivity analysis of a continuous tableting process is conducted via the wet granulation route (Metta et al., 2019). The modelling flowsheet consists of feeders, blenders, twin screw granulator (TSG), fluid bed dryer (FBD), comill and tablet press. These unit processes are connected sequentially and hereby the continuous modelling flowsheet is established where the step changes in API flow rate and dryer temperature are investigated. Whilst numerous modelling approaches such as data-

driven model, semi-empirical model, population balance model (PBM) and mechanistic model are used for the unit operations in the flowsheet, it was found that liquid feed rate in the granulator, the air temperature and drying time in the dryer are the main CPPs (Critical Process Parameters) affecting the tablet properties (De Leersnyder et al., 2018; Metta et al., 2019). Another example of a flowsheet model for a continuous process development for tableting is given (García-Muñoz et al., 2018), which consists of four subsystems i.e. the mixer, the vertical surge hopper, the transition piece and the feed frame. The selection criterion of the models in each subsystem is based on the physical understanding from the system and the necessity to account for the full spectrum of axial mixing behaviour with the least adjustable parameters.

Despite experimental studies of the twin screw granulator (Liu et al., 2018; Meng et al., 2019) and fluid bed dryer (De Leersnyder et al., 2018; Pauli et al., 2018) separately, the modelling study of the integrated TSG and FBD processes is rarely reported in the literature, let alone mechanistically sound model definition and proper model calibration and validation. Amongst the very few studies, the breakage and drying behaviour of granules in a continuous fluid bed dryer were experimentally investigated, which is mounted in a continuous manufacturing line

E-mail address: James.Litster@sheffield.ac.uk (J. Litster).

<https://doi.org/10.1016/j.ijpharm.2022.122186>

Received 7 April 2022; Received in revised form 2 September 2022; Accepted 3 September 2022

Available online 18 September 2022

0378-5173/© 2022 The Authors. Published by Elsevier B.V. This is an open access article under the CC BY license (<http://creativecommons.org/licenses/by/4.0/>).

Nomenclature

a	Fitting parameter, -
b	Fitting parameter, -
c	Fitting parameter, -
A_p	Surface area of particles, -
A_V	Particle surface area per volume fraction, -
A_{bed}	Cross-sectional surface area of bed, -
$B(v, t)$	The functions to denote the birth of particles, -
B_{nuc}	Nucleation rate, -
B_{CE}	Cumulative size distribution CEs, -
B_{KE}	Cumulative size distribution KEs, -
B_{x1}	Modified Weibull distribution, -
B_{x2}	Modified Weibull distribution, -
b_M	Breakage function, -
C_{LV}	The set of species in the vapour or liquid phases, -
C_V	The set of species present in the vapour, -
c_w	Heat capacity, -
$D(v, t)$	The functions to denote the death of particles, -
D_i	Diffusion coefficient, -
d_p	Particle diameter, -
\dot{F}_{in}	Inlet flow rates, -
\dot{F}_{out}	Outlet flow rates, -
F	Mass holdup, -
F_p^{in}	Inlet flow rate of phase p, -
F_p^{out}	Outlet flow rate of phase p, -
$f_b(x)$	Size distribution in the drying cell, -
G_m	Maximum growth rate, -
H_p	Total enthalpy holdup in phase p, -
$h_{i,p}^{in}$	Specific enthalpy of phase p in the inlet stream, -
$h_{i,p}^{out}$	Specific enthalpy of phase p in the outlet stream, -
$\Delta H_{drying,i,p}$	Enthalpy change rate resulting from drying, -
j_i	Mass flux of species i, -
k	Fitting parameters in Eq. (8), -
k	Granule compaction rate in Eq. (9), -
$k_{c,i}$	Mass transfer coefficient for species i, -
L	Bed height in the fluid bed dryer, -
$L_{in,powder}(x, t)$	Rate of liquid addition to the fine powder, -
M_{powder}	Mass of fine powder below the lower bound of the particle classes, -
$M_{granule}$	Mass of granule, -
$M_{i,p}$	Total mass holdup of species i in phase p, -
M_g	Gas mass, -
\dot{M}^*	Flux per unit z, -

$n(v, t)$	The number density function, -
P_b	Breakage probability, -
\dot{Q}	Heat flux, -
$R_{drying,i,p}$	Drying rate of phase p, -
R_{drying}	Drying rate, -
R_e	Reynolds number, -
S_M	Selection function, -
S_c	Schmidt number, -
S_h	Single particle Sherwood number, -
$Sh_{bulk,i}$	The bulk Sherwood number, -
T_w	Wall temperature, -
T_p	Particle temperature, -
T_g	Gas temperature, -
v	Vector representing particle property, -
ν_i	Normalised single particle drying rate, -
$V_{droplet}$	Volume of a single liquid droplet, -
X	Dry basis moisture content, -
X_c	Dry basis critical moisture content, -
X_{hyg}	Equilibrium moisture content, -
x_w	Moisture content, -
x_{wc}	Critical moisture content, -
$x_{i,p}^{in}$	Mass fraction of phase p in the inlet stream, -
$x_{i,p}^{out}$	Mass fraction of phase p in the outlet stream, -
$x_{vap,i}$	Mass fraction of species i in vapour phase, -
$x_{vap,j}$	Mass fraction of species j in vapour phase, -
Y_s	Moisture content in the suspension phase, -
$Y_{eq,i}$	Equilibrium of species i, -
$Y_{bulk,i}$	Bulk dry basis moisture content of species i, -
DYS	Dynamic yield strength, -
PFN	Powder feed number, -

Greek symbols

$\alpha_{s,g}$	Heat transfer coefficient between the solid and gas phase
τ	Residence time
ϵ	Granule porosity at time t, -
ϵ_{min}	Minimum porosity for consolidation to occur, -
η	Normalised particle moisture content, -
$\eta_p(r)$	Number of particles of radius r, -
$\eta_{flow,p}^{in}(r)$	Rate number of particles of radius r entering the unit, -
$\eta_{flow,p}^{out}(r)$	Rate number of particles of radius r exiting the unit, -
ρ_g	Density of gas phase, -
ϵ	The bulk Sherwood number correction, -
μ_g	Viscosity of the gas phase, -
μ_0	Superficial velocity of gas, m/s

(De Leersnyder et al., 2018). The moisture content of the granules produced from the upstream twin screw granulation is found to decrease with the increased drying time, air flow and drying temperature. The breakage and attrition of granules was observed due to pneumatic transfer of wet granules on the horizontal setup between the twin screw granulator and fluid bed dryer. However, the breakage and attrition behaviour are less significant in the vertical setup, but a higher degree of breakage and attrition is prone to occur when shorter drying times are applied. A two-step risk assessment of the twin screw granulation connected with fluid bed dryer was presented to identify and quantify the CPPs with regard to the CQAs (Critical Quality Attributes) (Pauli et al., 2018). The first step of the risk assessment is to generate a fishbone diagram listing all conceivable CPPs that can potentially have an influence on the CQAs. The second step is to identify the critical CPPs and uncritical CPPs based on the response from the CQAs. A key finding from the risk assessment is that most CPPs exert some influence on the granule

size distribution in TSG and moisture content in FBD simultaneously, making it difficult to control the CPPs independently from each other. These prior studies have greatly promoted the understanding of the integrated twin screw granulator and fluid bed dryer, from the perspective of experimental or statistical perspectives. Monaco et al. experimentally investigated the impact of drying time on the moisture content of granules, produced from twin screw granulation (Monaco et al., 2021). The drying time was found to linearly correlate with the amount of water present in a single cell of the segmented fluid bed dryer. The DoE-based experiments using a continuous high-shear granulator were performed to determine the key parameters affecting the tablet quality and productivity. The L/S ratio is identified as the key parameter on granule attributes e.g. density and flowability and tablet attributes e.g. disintegration and dissolution (Matsunami et al., 2020). The science-based digital twin, i.e. mechanistic model, is a computational method to employ process understanding with facilitated mechanisms to describe

and predict the quantitative behaviour of particulate systems for process design and optimisation, operational space exploration and tech transfer. Nevertheless, the science-based digital twin modelling of these unit operations is still lacking, which potentially jeopardises the implementation of Quality by Design (QbD) without the aid of science-based modelling framework. This is mainly because the experimental approach is restricted in the design space and the statistical approach falls short of the physical soundness in establishing the relationship between the CPPs and CQAs.

As an overture to attain a thorough understanding of the continuous manufacturing process, this paper focuses on the development of a digital twin, in the form of a science-based flowsheet modelling of an integrated twin screw granulation and fluid bed dryer. A recently proposed approach i.e. Model Driven Design (MDD), is adopted to reduce experimental design space, driven by the physics of the particulate processes (Wang et al., 2021a). To that end, the mechanistic models in the TSG and FBD are defined and the digital modelling platform for the integrated approach is established in gPROMS (gPROMS Formulated Products Release 1.6, 2020). The complementary experiments are carried out to provide a database with the least possible number of tests for model validation. Global System Analysis (GSA) is performed as the virtual design toolkit to extend the model prediction beyond the experimental scope and explore the process design space. The synergic effects of key CPPs on the CQAs, such as moisture content are discussed.

2. Model definition for TSG

2.1. Population balance model for TSG

The twin screw granulation has been extensively studied by means of population balance modelling (PBM) (Barrasso et al., 2015; Kumar et al., 2016; Liu et al., 2018; McGuire et al., 2019; Shirazian et al., 2019; Van Hauwermeiren et al., 2019). Amongst these studies, a distinct feature of the PBM for a twin screw granulation process is the proper definition of rate process kernels given the operational circumstances, such as the wide variety of liquid to solid ratios. Prior to the twin screw granulation mechanism proposed in this work, a general form of population balance model is first presented. For a well-mixed continuous TSG system, the population balance model used to simulate the granule attribute gives (Wang et al., 2021a):

$$\frac{\partial}{\partial t} n(v, t) + \frac{\partial}{\partial v} \left[n(v, t) \frac{dv}{dt} \right] = B(v, t) - D(v, t) + \dot{F}_{in} - \dot{F}_{out} \quad (1)$$

where $n(v, t)$ is the number density function; v is the vector representing particle property (herein volume); $B(v, t)$ and $D(v, t)$ are the functions to denote the birth and death of particles due to breakage and nucleation. \dot{F}_{in} and \dot{F}_{out} are the inlet and outlet flow rates in the TSG unit. Due to the fact that the rate processes are screw dependent in twin screw granulation, a compartmental approach is usually employed to solve a dynamic 1D population balance model.

As the screw configuration is a key contributor in the granule size distribution, a compartmental approach is usually opted to evaluate material transport along the barrel and each axial compartment is specified with an average residence time dependent on the screw elements. The inlet flow rate in one compartment is equal to the outlet flow rate in the last neighbouring compartment. It gives:

$$\dot{F}_{out} = \frac{F}{\tau} \quad (2)$$

where \dot{F}_{out} is the outlet flow rate for each compartment; F is the mass holdup and τ is the residence time in each compartment. It was worth mentioning that the residence time in kneading elements is found to be longer than that in the conveying elements. This is because of more congestion of powder and liquid phase mixing in the kneading elements. The inlet flow rate of a compartment is equal to the outlet flowrate of the

previous one. However, there is an exception for the first compartment where the inlet flow rate is specified based on the inlet feed rate of materials.

2.2. Model assumptions in TSG

The following key assumptions are made in the population balance modelling of TSG:

1. The screw element is well mixed and material flows in one direction alongside the granulator.
2. The residence time in each compartment is dependent on the screw element and its dimension, irrespective of the particle size and phases.
3. Liquid contained within the granule phase cannot be transferred to the fine powder or other granules. External liquid can contribute to the liquid content of granule phases when layering is assumed to occur.
4. Nucleation and layering contribute to the growth of the granule by means of depletion of fine powders. The size distribution of fine powders in the depletion is equal to that defined in the system. Layering is assumed to take place in both CE and KE whilst nucleation in only defined in CE.
5. The breakage mechanisms are dependent on the screw elements. The conveying element is dominant by chipping whilst the kneading or distributive mixing elements are dominant by fragmentation.
6. No chemical reaction and dissolution of fine powders and granules are considered. The screw temperature is operational using a constant value and doesn't have any influence on the granule size distribution.

The above assumptions for TSG are the same as our previous publication (Wang et al., 2021a).

2.3. Rate process kernels for TSG

The success of model-based predictive analysis for TSG is mainly dependent on the properly defined granulation rate process. Hagrahy and Litster studied the granulation rate process in the twin screw granulator where the conveying elements are configured with different sets of kneading elements (El Hagrahy and Litster, 2013). With numerous configuration parameters, i.e. kneading element length, the advance angle and the angle direction, it was observed with two main rate processes in the kneading elements: 1. Breakage followed by layering 2. Shear elongation and breakage, followed by layering. The granulation rate processes proposed for a configuration of conveying and kneading elements in TSG are shown in Table 1, which is the basis for the definition of the granulation rate kernels in this work.

Regarding the conveying elements, the agglomerates are created by drop-granulation due to the liquid dripping into the barrel. Then the agglomerates result in the depletion of fine powders by means of a layering mechanism. When the L/S ratio is increased to a higher value, it results in a higher likelihood of coalescence. As for the kneading elements, the CQAs of adding more kneading elements in the screw configuration are characterised by the liquid distribution and granule growth. The influence of adding more kneading elements on the granule properties can be categorized as: not applicable, positive change, negative change and no change. The kneading elements improve the liquid distribution excluding the forward 60°. The reverse direction is more likely to produce larger granules as compared to neutral and forward direction. The proposed granulation rate processes explain the underlying mechanism for the granule evolution within the TSG, furthermore they provide a framework for the rate kernel definition in population balance model. Detailed equations of rate process kernels of TSG used in the present work are presented in Appendix.

Table 1
Proposed granulation rate processes in a twin screw granulator (El Hagrasy and Litster, 2013).

Screw Type	Dominant Processes	More KE	
		Liquid Distribution	Granule Growth
Conveying	Drop Nucleation (DN)	NA	NA
	Layering	NA	NA
	High L/S Ratio Droplet Coalescence		
Neutral	Breakage	+	-
	Layering		
Reverse	30° Shear-Elongation and Breakage	+	+
	60° Layering		
Forward	30° Breakage + Layering + Conveying characteristics	+	+
	60° Conveying characteristic	Nil	Nil

NA: Not applicable + Positive Change - Negative Change Nil: No Change

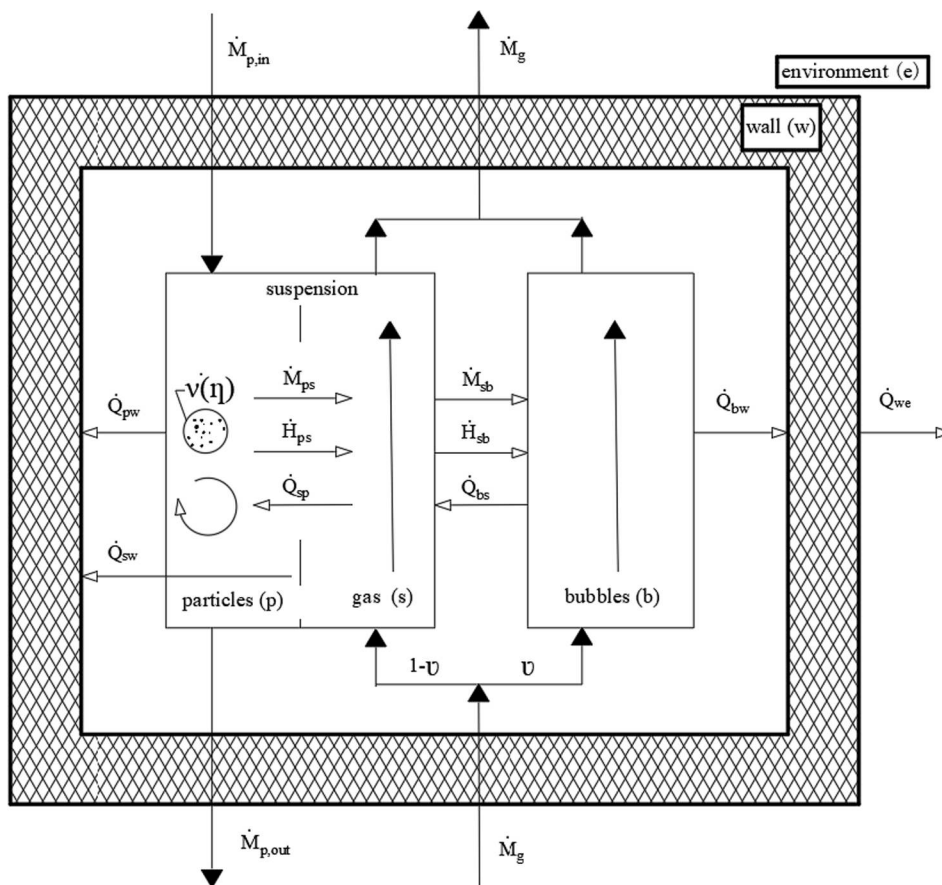


Fig. 1. Schematic of continuous fluid bed drying process (Burgschweiger and Tsotsas, 2002).

3. Model definition for FBD

Numerous mechanistic studies of drying processes for wet porous granules have been attempted in the fluid bed dryer. A review of mechanistic modelling in fluidized bed drying presents the comparison of different modelling techniques such as PBM, CFD (Computational Fluid Dynamics) and the coupling of PBM-CFD (Mortier et al., 2011). The PBM describes the behaviour of a population of particles whereas the CFD model describes the fluid dynamics such as the multiphase flow of particle and gas. Given a spatially heterogeneous system, coupling of the PBM-CFD models considers spatial information of multiphase medium. The selection for a specific modelling or coupling approach is strongly dependent on the intended objective. The objective of this section is to develop a coupled population balance and drying model to calculate the dynamic evolution in the moisture content of particles in FBD.

3.1. Model assumption in FBD

A schematic of the governing mechanism for a continuous fluid bed drying process is shown in Fig. 1, which is adopted from the model of (Burgschweiger and Tsotsas, 2002). Before a detailed description of key equations in this model is given, the main assumptions for the Burgschweiger and Tsotsas model (Burgschweiger and Tsotsas, 2002) are listed below:

1. Particle elutriation is not considered.
2. Accumulation of solid and vapour in the unit is considered.
3. The unit is perfectly mixed and spatial heterogeneity is not considered.
4. The particle and gas phases are both perfectly mixed and the gas phase is not distinguished into the suspension and bypass bubble phases.
5. Particle drying abides by the falling rate kinetics. The drying process only allows for the creation of intra-particle void space. Shrinkage of particles due to drying is not considered.

It should also be noticed that the perfect back mixing of particles in the suspension phase consists of both the vertical and horizontal direction.

3.2. Mass and energy balance in the solid phase

Given a perfect mixing unit without chemical or nuclear reactions, the change rate of any species within the unit can be expressed by.

$$\frac{dM_{i,p}}{dt} = F_p^{in} x_{i,p}^{in} - F_p^{out} x_{i,p}^{out} - R_{drying,i,p} \quad (3)$$

where $M_{i,p}$ is the total mass holdup of species i in phase p ; F_p^{in} and F_p^{out} are the inlet and outlet flow rate of phase p ; $x_{i,p}^{in}$ and $x_{i,p}^{out}$ are the mass fraction of phase p in the inlet and outlet stream; $R_{drying,i,p}$ is the drying rate of phase p which is lost to the vapour phase.

As for the energy balance for the particle phase, it is assumed that the pressure is constant in the unit and the contents in the unit are incompressible. Likewise, the rate of energy accumulation is given by:

$$\frac{dH_p}{dt} = F_p^{in} h_{i,p}^{in} - F_p^{out} h_{i,p}^{out} - \Delta H_{drying,i,p} \quad (4)$$

where H_p is the total enthalpy holdup in phase p in the unit; $h_{i,p}^{in}$ and $h_{i,p}^{out}$ are the specific enthalpy of phase p in the inlet and outlet stream; $\Delta H_{drying,i,p}$ is the enthalpy change rate resulting from drying.

Unlike the population balance equation in TSG, there are no particle evolution kernels, i.e. agglomeration and breakage defined in the fluid bed dryer. The evolution of particle size distribution is only governed by the inlet and outlet flow rate and it can be given as:

$$\frac{\partial \eta_p(r)}{\partial t} = \eta_{flow,p}^{in}(r) - \eta_{flow,p}^{out}(r) \quad (5)$$

where $\eta_p(r)$ is the number of particles of radius r in the unit; $\eta_{flow,p}^{in}(r)$ and $\eta_{flow,p}^{out}(r)$ are the rate number of particles of radius r entering and exiting the unit respectively.

3.3. Mass and energy balances for the vapour phase

The mass balances of vapour in a control volume in the vapour phase can be derived as.

$$\frac{dM_{i,v}}{dt} = F_v^{in} x_{i,v}^{in} - F_v^{out} x_{i,v}^{out} + R_{drying,i,v} \quad (6)$$

where $M_{i,v}$ refers to the total mass of species i in the vapour phase v ; F_v^{in} and F_v^{out} are the inlet and outlet flow rate of vapour phase v ; $x_{i,v}^{in}$ and $x_{i,v}^{out}$ are the mass fraction of vapour phase v in the inlet and outlet stream; $R_{drying,i,p}$ is the drying rate of phase p which is lost to the vapour phase.

Analogue to the mass balance, the energy balance of the vapour phase gives:

$$\frac{dH_v}{dt} = F_v^{in} h_{i,v}^{in} - F_v^{out} h_{i,v}^{out} + \Delta H_{drying,i,p} - \dot{Q}_{pw}^* - \dot{Q}_{vw}^* \quad (7)$$

where H_v is the total enthalpy in the vapour phase; $h_{i,v}^{in}$ and $h_{i,v}^{out}$ are the specific enthalpy of the vapour inlet and outlet stream; \dot{Q} is the heat flux and the subscript of \dot{Q} indicates the interaction between the phases of particle, vapour and wall.

The energy balance for the wall is determined as.

$$c_w \frac{dT_w}{dt} = \dot{Q}_{pw} + \dot{Q}_{we} - \dot{Q}_{wv} \quad (8)$$

given that c_w is the specific heat capacity and T_w is the wall temperature. The subscript p , W and e of \dot{Q} indicates the interaction between the phases of particle, wall and environment.

3.4. Drying equations

3.4.1. Drying rate

The drying rate for any given solid phase is given as.

$$R_{drying} = A_p \cdot j_i \quad i \in C_{LV} \quad (9)$$

where R_{drying} is the drying rate; A_p is the surface area of particles exposed for drying; j_i is the mass flux of species i and C_{LV} is the set of species in the vapour or liquid phases for vaporisation.

The mass flux j_i in Eq. (9) is calculated as.

$$j_i = \nu_i \rho_g k_{c,i} (Y_{eq,i} - Y_{bulk,i}) \quad i \in C_{LV} \quad (10)$$

where ν_i and ρ_g are the normalised single particle drying rate and the density of gas phase; $k_{c,i}$ is the mass transfer coefficient for species i ; $Y_{eq,i}$ and $Y_{bulk,i}$ are the equilibrium and bulk dry basis moisture content of species i in the gas phase respectively.

The bulk dry basis moisture content gives:

$$Y_{bulk,i} = \frac{x_{vap,i}}{\sum_{j \in C_V - C_{LV}} x_{vap,j}} \quad (11)$$

where $x_{vap,i}$ and $x_{vap,j}$ are the mass fraction of species i and j in vapour phase; C_V is the set of species present in the vapour phase whilst C_{LV} is the set of species in the vapour and liquid phases which are able to vaporise.

The normalised drying rate is defined as the ratio of actual drying rate \dot{Q}_{ps} and the drying rate $\dot{Q}_{ps,I}$ in the first drying period for hygroscopic materials (Peglow et al., 2007),

$$\dot{v}(\eta) = \frac{\dot{Q}_{ps}(\eta)}{Q_{ps,l}(\eta)} \quad (12)$$

the normalised particle moisture content η is.

$$\eta = \frac{X - X_{hyg}}{X_c - X_{hyg}} \quad (13)$$

where X is the dry basis moisture content; X_c and X_{hyg} are the dry basis critical moisture content and equilibrium moisture content.

3.4.2. Determination of mass and heat transfer coefficients

There are several means for the determination of mass and heat transfer coefficients (Fries et al., 2011; Poós and Szabó, 2021). In this work, the Burgschweiger and Tsotsas model (Burgschweiger and Tsotsas, 2002) is chosen considering the externally limited drying regime.

The heat transfer between the fluidised gas and the particles is defined as:

$$\dot{q}_{s,e,k} = \alpha_{s,g} \frac{\pi}{6} \int_0^\infty x^2 f_b(x) (T_p - T_g) \quad (14)$$

where $\alpha_{s,g}$ is the heat transfer coefficient between the solid and gas phase, $f_b(x)$ is the size distribution in the drying cell whilst T_p and T_g are the particle and gas temperature, respectively.

The mass transfer coefficient $k_{c,i}$ is calculated from the bulk Sherwood number as below:

$$Sh_{bulk,i} = \frac{k_{c,i} d_p}{D_i} i \in C_{LV} \quad (15)$$

where $Sh_{bulk,i}$ is the bulk Sherwood number; d_p and D_i are the particle diameter and diffusion coefficient of species i .

The bulk Sherwood number $Sh_{bulk,i}$ is given by.

$$Sh_{bulk,i} = \frac{\epsilon R_e S_c}{A_V L} \ln \left(1 + \frac{A_V L S_h}{R_e S_c} \right) \quad (16)$$

where ϵ and R_e are the bulk Sherwood number correction and Reynolds number; S_c and S_h are the Schmidt number and single particle Sherwood number, respectively. A_V and L are the particle surface area per volume fraction and bed height in the fluid bed dryer. Note that the total surface area of particles A_p and cross-sectional surface area of bed A_{bed} are used instead to express the combined effect of A_V and L . Their equilibrium is given as $A_V L = \frac{A_p}{A_{bed}}$.

Note that the strength of Eq. (16) is that the bulk Sherwood number can be calculated instead of estimation or adaption.

And the single particle Sherwood number Sh is expressed as a function of Reynolds number Re_o and Schmidt number Sc_i and gives.

$$Sh = 2 + 0.6 Re_o^{1/2} * Sc_i^{1/3} \quad (17)$$

The Schmidt number Sc_i is given as.

$$Sc_i = \frac{\mu_g}{\rho_g D_i} i \in C_{LV} \quad (18)$$

where $\mu_g = \sum_{i \in C_V} X_{vap,i} \mu_{vap,i}$ is the viscosity of the gas phase.

The Reynolds number is give as (Peglow et al., 2007):

$$Re_o = \frac{d_p \mu_0 \rho_g}{\mu_g} \quad (19)$$

where $\mu_0 = \frac{M_g}{\rho_g A_{bed}}$ denotes the superficial velocity of gas.

The details of heat transfer will not be expanded herein but can be found elsewhere (Burgschweiger and Tsotsas, 2002).

4. Experimental protocol

This experimental protocol is proposed to provide the database generated from least possible amount of experiments for the model

validation of the aforementioned integrated TSG and FBD processes. The DiPP (Diamond Pilot Plant), a continuous powder process plant installed at the University of Sheffield, is employed in the experimental design for the data measurement required in the model validation. The DiPP is an integration of the complete ConsigmaTM-25 production and ModuleP tablet press line for manufacturing of formulated products and has a series of unit operations working simultaneously from powder to tablet compaction line (Wang et al., 2021b). It consists of twin screw granulator, fluid bed dryer, cone mill, vertical blenders and tableting rotary press. The DiPP features a modular approach which allows for the customized modules to suit specific needs. For instance, this section presents the experimental study of the first two-unit operations in DiPP for the purposeful process of granule enlargement and drying respectively.

4.1. Integrated TSG and FBD

Despite a unique continuous production line from powder to tablet in DiPP, this work is focused on the integrated TSG and FBD as shown in Fig. 2. In Fig. 2a, the granulation module in the ConsigmaTM-25 DiPP comprises an overhead hopper and a loss-in-weight feeder with a pair of twin screw assemblies. The hopper and the feeder serve to deposit the blended powder and transport it to the TSG. The blended powder is further transported via the conveying elements and mixed at a port where liquid is injected as a binder for nucleation. The wet agglomerates are then intensively mixed using the kneading elements with dominant mechanisms of breakage and layering as stated in Section 2.3. The wet granules are gravimetrically transported to the fluid bed dryer consisting of six segments through a rotating inlet valve.

The six segmented cells in FBD are sequentially fed with wet granules for a set loading time and start drying at the set drying conditions. Once the loading time is finished, the wet granules are directed to the next cell whilst the previous cell continues the drying process for the set drying time. Once the drying time finishes, the dried granules are then conveyed pneumatically to the Granule Conditioning Unit (GCU). In the GCU, the granules are milled and blended with extra materials before going through the final tableting stage, which is beyond the scope of investigation for this work and will not be expanded for discussion. The integrated TSG and FBD can be automated, gauged and monitored with several key parameters through the control/ monitoring panel. For example, the torque applied on the screw and the barrel temperature are monitored through the monitoring panel and the real-time data are saved for further analysis. An NIR spectrometer (Near Infra-Red, Fibre Optic FP710e, NDC Technology, Essex, UK) is mounted in one segment of the fluid bed dryer to monitor the moisture content of the granules in real-time. The data collection and transfer are carried out by the monitoring panel. Fig. 2b schematically depicts the working principle corresponding to the integrated TSG and FBD shown in Fig. 2a. The time-controlled valve is placed at the bottom of the cells to discharge the dried granules to the downstream GCU (Granule Conditioning Unit).

4.2. Materials and operational condition

The blending of the powders for the integrated TSG and FBD flow-sheet was carried out beforehand in a 20L batch Tumbler Mixer (Inversina Tumbler Mixer, Wald, Switzerland). After each time of blending, the blend is sieved with a mesh size 1 mm sieve to avoid any potential agglomeration of clustered powders. The blended powder is composed of 72 % lactose (DFE Pharma, Germany), 24 % MCC and 4 % PVP (Harke Pharma GmbH, Germany). Distilled water was used in this study as a binder.

The twin screw granulation was carried out at a constant feed rate of 10 kg/h and screw speed of 500 RPM. The barrel temperature was set to 25 °C and the L/S ratio (Liquid to solid ratio) is varied from 0.15 to 0.35 with an interval of 0.05. The screw configuration is composed of 8 compartments, including 5 compartments of conveying elements and 3

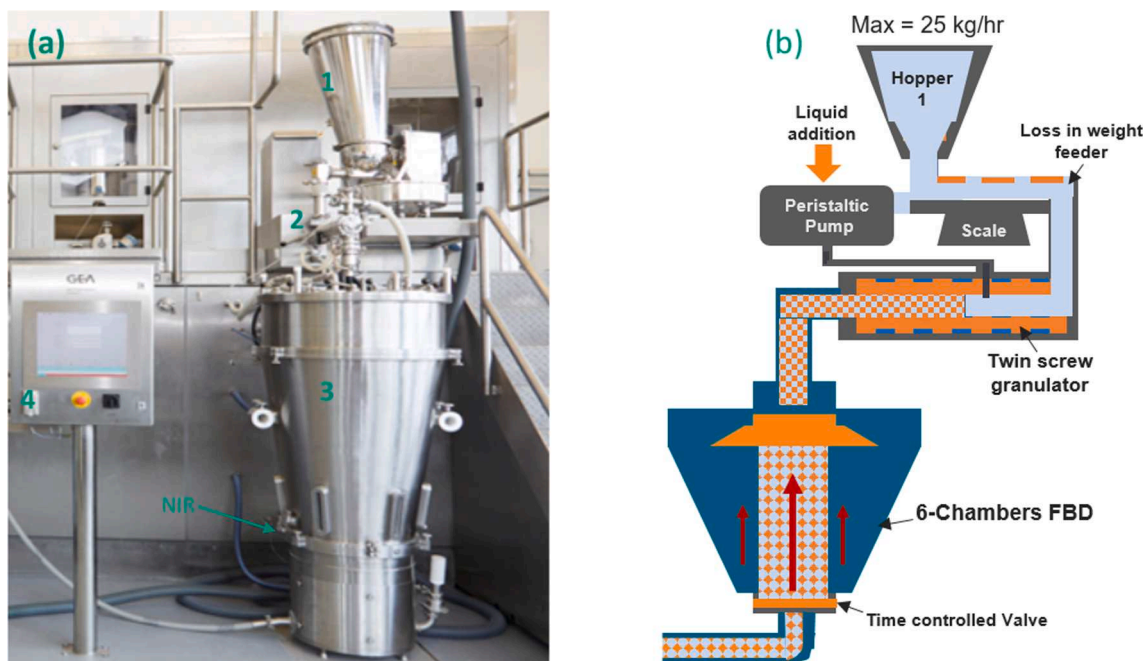


Fig. 2. (a) The modular assemble of integrated TSG and FBD in DiPP (1. Hopper 2.Twin screw granulator 3. Six-segment Fluid bed dryer 4. Monitoring panel) and (b) the schematic of the corresponding powder process.

compartments of kneading elements as shown in Fig. 3. In compartment 2, only nucleation is assumed to happen due to the injection of liquid droplet. The third, fifth and seventh compartments are conveying elements where breakage (chipping) and layering are the dominant mechanism. The fourth, sixth and eighth compartments are kneading elements where consolidation is the additional mechanism apart from breakage (fragmentation) and layering. Due to the varying intensity of stressing events in conveying and kneading elements, the model parameters for the breakage rate and layering rate are not expected to be the same.

The length to diameter ratio for the granulator is 25:1. The stagger angle of kneading elements is 60° and the first and second compartments of KE is subdivided with 6 blocks of kneading element (6.25 mm in length). Before starting the granulation in the TSG, the fluid bed dryer is preheated to the intended drying temperature with a constant airflow rate of 360 m³/h. The filling time for each cell is set to 240 s. The drying stage takes 660 s and totals 900 s as a full drying cycle. At the end of

drying stage, the dry granules are discharged using a pneumatic conveyor system.

4.3. Critical process parameters and critical Quality attributes

The CQAs are usually dependent on the CPPs in a given unit operation. An evaluation of CPPs identifying their influences on the CQAs is typically required in order to find the optimal process conditions and product attributes. Nonetheless, traditional ways of evaluation are carried out by trial-and-error from the heuristic data (Fonteyne et al., 2013). Furthermore, such evaluation process is time- and product-consuming and cannot guarantee finding the optimal solutions, it is recommended by an organized method such as DoE (Design of Experiments) to establish the relationship between CPPs and CQAs (Fonteyne et al., 2013; Liu et al., 2019). It was found that the powder feed rate (10–25 kg/h) and barrel temperature (25, 32.5 and 40 °C) had significant effects upon the granule size in TSG (Fonteyne et al., 2013). In

	Powder	Liquid						
Compartment	1	2	3	4	5	6	7	8
Type	CE	CE	CE	KE	CE	KE	CE	KE
Length [mm]	112.5	50	150	37.5	37.5	37.5	37.5	8
Angle (°)	0	0	0	60	0	60	0	60
Rate process kernels	NA	Nucleation	Breakage Layering	Breakage Layering Consolidation	Breakage Layering	Breakage Layering Consolidation	Breakage Layering	Breakage Layering Consolidation

Fig. 3. Screw configuration of Consigma™-25 twin screw granulation.

contrast, the barrel temperature (30–40 °C) in TSG was found to be uncritical on the PSD through DoE (Pauli et al., 2018). The disagreement of barrel temperature effect on the granule size can be accounted with differing combination of CPPs. Another DoE study of TSG using Box-Behnken method was presented to investigate the influence of process parameters, e.g. screw speed and screw configuration on granule properties and tablet properties (Liu et al., 2019). As CQAs are essential elements in the QbD (Quality by Design) (Yu et al., 2014), Table 2 summarizes the CQAs in the twin screw granulation and fluid bed dryer. As for the CPPs in this work, it is not intended to exhaustively investigate their effects on the CQAs. Instead, only the most influential CPPs in TSG and FBD, i.e. L/S ratio and air temperature are selected and the design space will be explored based on a successful model validation with the provided dataset.

4.4. Characterisation of granule properties

In order to investigate the effect of the CPPs in the TSG on granule size, the wetted granules were collected from the exit of TSG and dried overnight at the room temperature of DiPP (22 °C) before the granule size distribution characterisation. The granule size distribution was measured using a Retsch VE 1000 sieve shaker using a series of screen sizes (63, 90, 125, 180, 250, 355, 500, 710, 1000, 1400, 2000, and 2800 μm). The sieves were shaken subject to an amplitude of 0.76 mm within an interval of every 20 s for total of 1 min. The amount of retaining granules on each sieve is scaled and the granule size distribution is plotted as a function of mass-based density. The granule moisture content is measured using the NIR probe, which is calibrated beforehand using LOD measurement (MA35, Satorius GA, Germany), where 10 samples with varying moisture content ranging between 0 % and 35 % are deployed to benchmark the drying curve. The air temperature in the FBD is varied as 40 °C, 50 °C, 60 °C, and 70 °C to measure their influence on the moisture content whilst the humidity and airflow rate were kept constant.

4.5. Results and discussion

4.5.1. L/S ratio on granule size distribution in TSG

The effect of L/S ratio on the final size distribution of granules has been extensively studied. Generally increasing the L/S ratio results in a higher d_{50} and lower d_{10} while the granule size distribution is shifted to a narrower and monomodal size distribution (Dhenge et al., 2010). Fig. 4 shows the granule size distribution as a function of L/S ratio for the formula in the screw configuration. The proportion of granules increases alongside the increase of L/S ratios. Under the L/S ratios of 0.15 and 0.20, the peak granule proportion arrives at the size interval of 1000 μm. When the L/S ratios is increased from 0.20 to 0.35, the peak

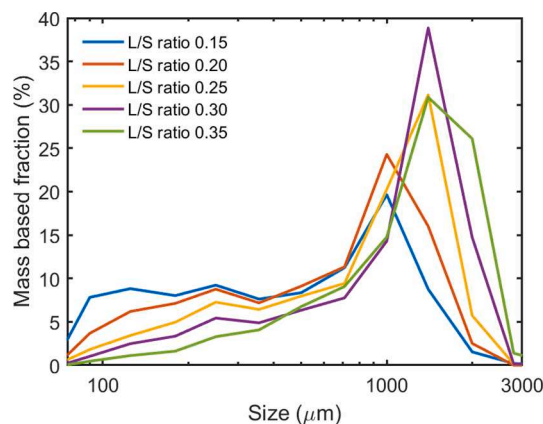


Fig. 4. Granule size distribution in TSG with differing L/S ratios.

granule proportion is shifted right side and arrives at 1400 μm. The shift of the whole granule size distribution under increasing L/S ratios was also observed for the lactose within previous experimental studies of another screw configuration including conveying elements and kneading elements (El Hagrasy et al., 2013). The granule size distribution curve is increasingly shifted from bimodal into monomodal when the L/S ratios are increased. Specifically, the monomodal can be clearly observed in the highest L/S ratio of 0.35. Such observation is in accordance with the literature report where a higher L/S ratio results in a narrower, monomodal size distribution (Dhenge et al., 2010; El Hagrasy et al., 2013).

4.5.2. Air temperature on moisture content in FBD

The effect of air temperature on moisture content in the segmented fluid bed dryer is shown in Fig. 5. A dashed line is drawn vertically in Fig. 5 as demarcation to distinguish the loading stage of wet granules until 240 s and then the drying stage until 900 s. In the loading stage, the moisture content increases sharply in the first 25 s due to the accumulation of wet granules exiting from the twin screw granulator on the NIR probe. As the fluid bed dryer is preheated, the moisture content decreases until 80 s prior to the stable increase at the end of 240 s. The final value of moisture content at the 240 s is found to decrease with the increase of air temperature. When the loading is completed, the moisture content is seen to diminish increasingly quickly with regard to the increase of air temperature. The increase of air temperature from 40 °C to 70 °C results in a faster drying and a lower value of moisture content for wetted granules. The moisture content of granules continues to

Table 2
Summary of CPPs and CQAs in the twin screw granulator and fluid bed dryer.

Unit Operation	Critical Process Parameters (CPPs)	Critical Quality Attribute (CQAs)	Method to quantify CQAs
Twin screw granulation	L/S ratio (Liquid to solid ratio)	Granule size distribution	Sieve analysis (El Hagrasy et al., 2013)
	Powder feed number	Porosity	Helium pycnometer (El Hagrasy et al., 2013)
	Screw speed		
	Barrel temperature		
	Binder type/concentration		
Fluid bed dryer	Residence time distribution		
	Drying time	Moisture content	NIR (Fonteyne et al., 2014)
	Loading time		
	Air temperature		
	Air flow rate		
	Elutriation rate		

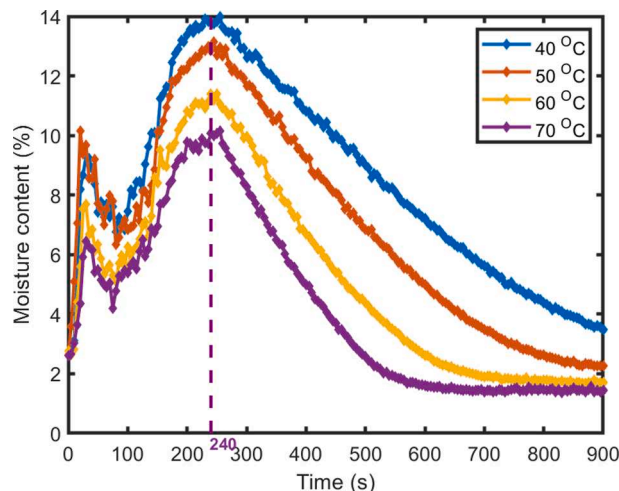


Fig. 5. Moisture content evolution over full drying cycle.

decline at the endpoint of drying stage. Nevertheless, the moisture content of granules at 60 °C to 70 °C starts to level off at a constant value from 750 s and 650 s respectively. Such trend was generally in good agreement from the literature regarding the effect of air temperature (De Leersnyder et al., 2018).

5. Model validation and predictive analysis

5.1. Digital modelling platform of integrated flowsheet

There are separate built-in modules of twin screw granulator model and fluid bed dryer model in gPROMS FormulatedProducts, which are designed to simulate the wet granulation and drying processes respectively. In this study, the breakage kernel in TSG is customized whilst the other kernels are default in the standard library. Fig. 6 depicts the integrated flowsheet of the twin screw wet granulation and fluid bed drying. The digital module of the integrated flowsheet consists of the global specifications, the simulation duration, the powder and liquid specification and the twin screw granulator for the setup of rate process kernels, and the vapour source, the fluid bed dryer for the setup of drying mechanism, the moisture content sensor, vapour sink and blank outlet.

The module of global specification defines the minimum and maximum particle distribution for the feed powder and final granule, as well as the grid number of size in consideration. The simulation duration specifies the duration of the dynamic simulation for the integrated flowsheet. The module of powder and liquid specification sets up the material properties such as bulk density, intra-particle void fraction, and the PSD as well as the flow rate. The module of twin screw granulator is the most important part in which the screw configuration, the rate processing kernels and the initial conditions of powder and liquid are defined. The TSG module mainly includes three parts of information for model definition. The first part is the screw configuration based on the screw element types; The second part is the definition of rate process kernels including nucleation, breakage, layering and consolidation; The third part is the specification of initial conditions such as mass composition and size distribution of granules to define whether composite

granules pre-exist in the granulator. Note that all the rate processing kernels specified in the platform of gPROMS FormulatedProducts have been summarised in the aforementioned sections.

As regard to the section of fluid bed drying, the vapour source model provides the input value for the vapour composition, the vapour flow rate and operational conditions such as the pressure and the air temperature. The model of vapour sink is to represent the ending point of vapour stream in the flowsheet and to provide detailed vapour information. It is hypothesized that the vapour sink has infinite volume so as to accept the whole amount of vapour in the specified simulation duration. The outlet of the fluid bed dryer is connected with blank outlet, which act as the virtual downstream process and is essential an empty sink. The moisture content sensor is used to monitor the real-time variation of moisture content in the modelling duration and can provide both overall moisture content and the moisture distribution spanning the particle size distribution of the solid phase. The model of the segmented fluid bed dryer is most critical part to configure the dimension of the FBD, any potential drying mechanism such as drying model selection, elutriation and agglomeration, and the schedule of drying stages. Only drying is assumed to take place in this process and the drying model is based on (Burgschweiger and Tsotsas, 2002), which is outlined in Section 3.

5.2. Numerical solver and parameter estimation

The model definition in the TSG and FBD consists of a series of partial differential and algebraic equations (PDAEs), describing the size, mass and energy balances. The numerical solver of DAEBDF (Differential Algebraic Equation Backward Differentiation Formulae) is used to solve the resulting PDAEs, which is designed to deal with large, sparse systems of equations. Another solver of MXLKHD (Maximum likelihood) in gPROMS is specifically designed to search for the best possible fitted model parameter values via parameter estimation where the most influential parameters are selected in the defined equations. The MXLKHD solvers is based on a sophisticated sequential quadratic programming (SQP) method to find the global optimum. The MXLKHD is an indirect solver as the objective function gradient with respect to the

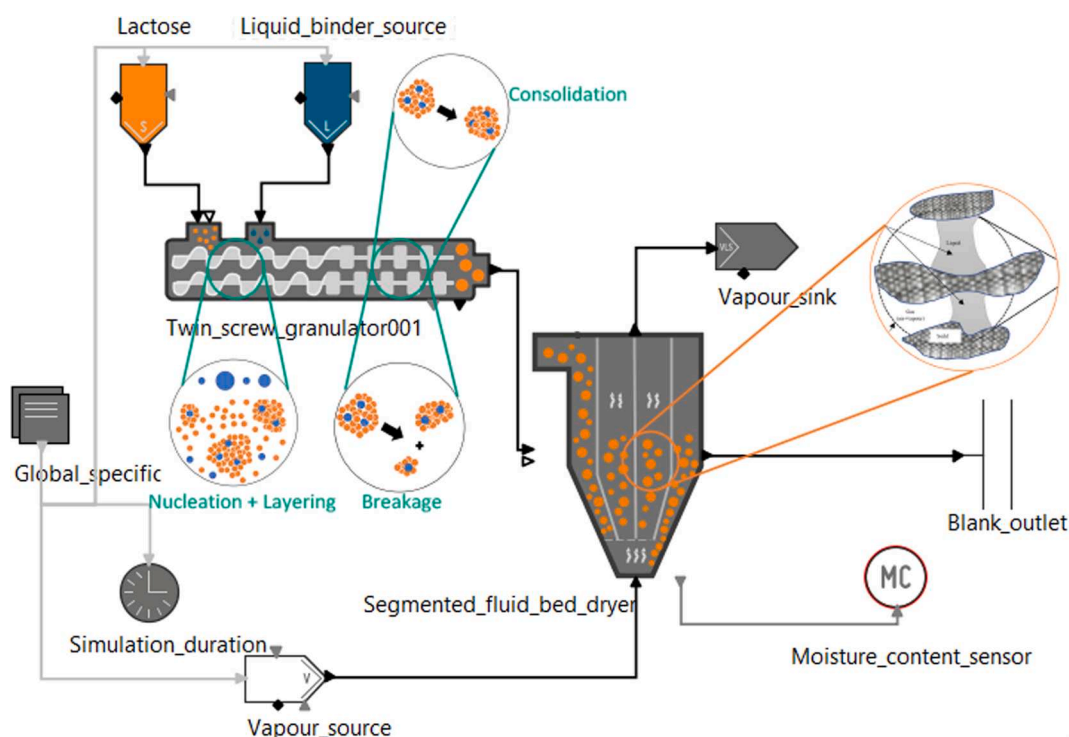


Fig. 6. Modelling flowsheet of integrated TSG and FBD in gPROMS FormulatedProducts.

selection parameters is calculated and the first order derivative information is used to determine the search direction. More details about the numerical solver DAEBDF and the algorithm MXLKHD have been clearly explained elsewhere (“gPROMS Formulated Products Release 1.6,” 2020).

5.3. Model calibration and validation

Model calibration and validation are a critical step to form a predictive capacity of CQAs in the defined model based on the comparison to the experimental data. Model calibration is usually carried out first to find the optimal values of the parameters for estimation, with which the model is able to produce acceptable closeness as contrasted to the experimental dataset. Model validation is further performed to ensure the defined model with calibrated parameters can predict the accurate results compared to the external dataset or beyond the existing experimental scope. Prior to the model calibration and validation, the input parameters of the defined models in TSG and FBD are first summarized and followed by selecting the key parameters for optimum via parameter estimation in gPROMS for model calibration and validation.

5.3.1. Input parameters

A defined list of these input parameters as well as the initial input values are summarized in Table 3. The category of these parameters has

Table 3
Defined list of PBM reference input parameters for TSG in gPROMS.

Category	Input Parameter	Method to quantify	Input Value
Rate parameters (Nucleation)	Mean droplet diameter	Estimate	1.0 mm
	Stdv of the droplet diameter	Estimate	0.45 mm
	Droplet pore penetration	Estimate	0.4 mm
Rate parameters (Breakage)	Breakage rate	Estimate	CE: 4.5 s-1 KE: 6 s-1
	Maximum critical size	Characterisation	CE: 3500 μ m KE: 3200 μ m
	Minimum critical size	Literature(Wang et al., 2020)	1000 μ m
	Dynamic yield strength		10 kPa
	Size exponent		CE: 2 KE: 10
	$a_{SF,CE}$		CE: 74.5
	$a_{SF,KE}$		KE: 0.0303
	$b_{SF,CE}$		CE: 0.41
	$b_{SF,KE}$		KE: 0.9
	Proportion		CE: 0.4 KE: 1.0
Rate parameters (Layering)	Scale parameter	Estimate	CE: 2.54e10 KE: 1.0
	Shape parameter	Estimate	CE: 9.3 KE: 1.48
	Layering rate constant	Literature (Barrasso and Ramachandran, 2016)	25 μ m/s
Rate parameters (Consolidation)	Critical moisture content	Estimate	0.2
	Kinetic parameter A	Estimate	10
	Kinetic parameter K	Estimate	0.2
Rate parameters (Consolidation)	Consolidation rate constant	Literature (Barrasso and Ramachandran, 2016)	0.002 s-1
	Minimum porosity	Estimate	0.2

already been classified from our previous work (Wang et al., 2021a). As seen in the table 3, three methods to quantify the values of input parameters i.e. Estimate, Characterisation and Literature are listed following the MDD approach. Majority of the input parameters have to be estimated or referred from the literature. The maximum critical size in breakage kernel is directly related to the screw geometry and can be directly measured as characterisation. For the nucleation and breakage kernel, majority of the input parameters are referred from our previous publication (Wang et al., 2021a); For the consolidation kernel, the input parameter values are referred from the publication of Barrasso and Ramachandran (2016).

The other categories of input parameters, i.e. the material parameters, TSG parameters and process parameters have been mentioned in Section 4.

The average residence time value is defined as 0.051 s/cm and 0.089 s/cm as referred to our previous work (Wang et al., 2021a).

The key input parameters in the FBD are summarized in Table 4. Comparatively, the input parameters in FBD are less than those in TSG as only drying model is considered. The initial condition of FBD is enabled as the FBD is preheated in the DiPP prior to the loading of wetted granule in the segmented cell.

With the input parameter summarized in Table 3 and Table 4, model verification must be performed to ensure the digital modelling flowsheet of integrated TSG and FBD is producing reasonable results. When the model verification is completed, the model calibration and validation of the modelling flowsheet are described below.

5.3.2. Model calibration and validation in TSG

The three L/S ratios, 0.15, 0.25, 0.35 are selected for the model calibration whilst the other two L/S ratios 0.20 and 0.30 will be used as external data for model validation to test the predictive capacity of the calibrated model. Table 5 lists standard deviation and maximum pore saturation in nucleation, the breakage rate in CEs and KEs, the proportion in CEs, the selection and Weibull parameters in CEs, layering rate for parameter estimation. In total, there are eight parameters for estimation and the optimized value for these parameters are achieved through the MAXLHD in gPROMS. The reason for selecting these parameters is based on the sensitivity analysis that nucleation and breakage are the key mechanisms in TSG (Wang et al., 2021a). In addition, the layering rate is used to establish the relationship with L/S ratios. This is supported by the previous work that the amount of coarse granules increases with higher L/S ratio and large granules have a higher liquid content related to L/S ratio (Sayin et al., 2015). A simple linear relationship is assigned as $G_m = a + b \cdot L/S_{ratio}$ and the initial values of a and b given in Table 5.

The result of model calibration with the optimized value for estimated parameters is shown in Fig. 7. The fitted granule size distribution shows strong agreement with the experimental data under the L/S ratios 0.15, 0.25 and 0.35. Despite an underestimation of the peak proportion of granules at 1400 μ m, the fitted results successfully capture the transition of bimodal to monomodal when increasing the L/S ratios. This transition is observed by the increasingly flattening curve of fine powders as well as the narrower granule size curve.

Table 4
Input value of key parameters in the defined model for FBD.

Input parameters	Input values	Unit
Cross-sectional area	0.2	m^2
Single segment volume	0.035	m^3
Critical moisture content (Dry-basis)	1.0	%
Bulk Sherwood correction	0.4	Dimensionless
Relative humidity in vapour	1.0	%
Mass fraction, Oxygen	0.2	kg/kg
Mass fraction, Nitrogen	0.8	kg/kg
Pressure	1.0	bar

Table 5
Selection parameters for model calibration in TSG.

Parameters for estimation (unit)	Initial value	Optimized value
Standard deviation of droplet (mm)	0.2	0.52
Maximum pore penetration (m ³ /m ³)	0.38	0.40
Breakage rate in CE (/s)	0.18	1.5
Breakage rate in KE (/s)	3.44	2.5
Proportion in CE	0.14	0.40
Scale parameter in CE	5.58e11	2.54e10
Weibull parameter in CE	5.26	8.23
Layering rate, a	1400	2715
Layering rate, b	-203	-202

The L/S ratios 0.20 and 0.30 are used as the external data to test the validity of the calibrated model. The comparison between the predicted granule size distribution from the TSG model and the measured value is shown in Fig. 8. The predicted granule size distribution agrees well compared to the external data. At 0.3 L/S ratio, the size of the distribution mode is underestimated, as is the case at the 0.25 and 0.35 calibration sets. Nevertheless, key properties of the distribution such as the d10, d50, and d90 are well predicted. This mismatch could be due to the presence of some coalescence at the higher moisture content, which is neglected in the model.

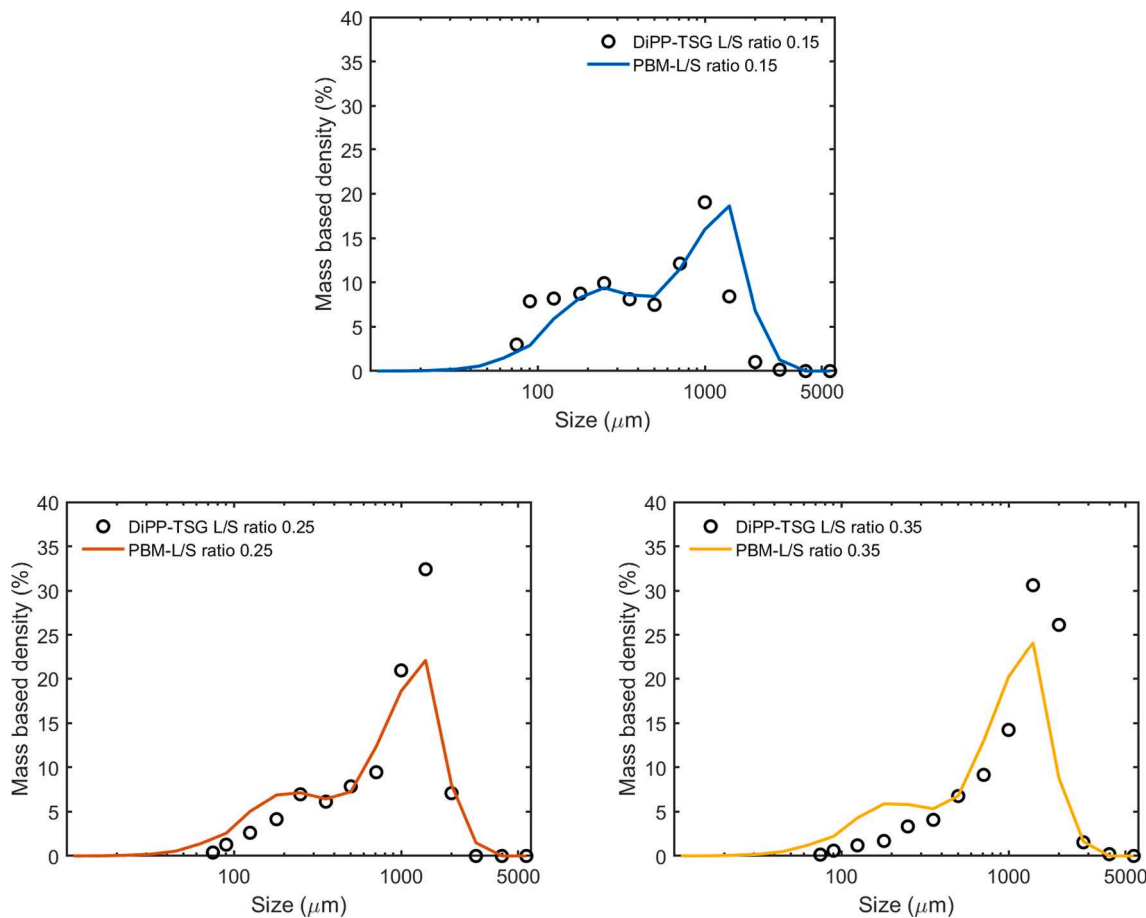


Fig. 7. Model calibration under L/S ratios 0.15, 0.25 and 0.35 for TSG.

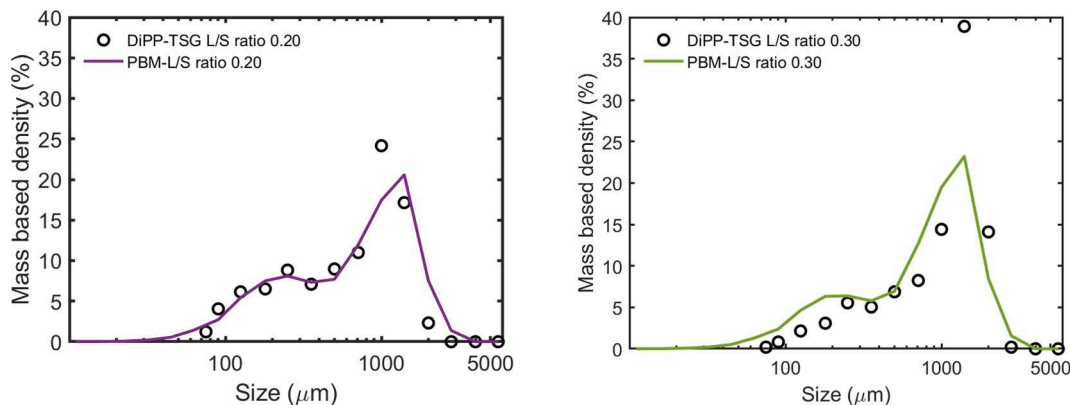


Fig. 8. Model validation under L/S ratios 0.20 and 0.30 in TSG.

5.3.3. Model calibration and validation in FBD

Analogous to the model calibration in TSG, the air temperature of 40 °C, 60 °C and 70 °C are chosen as the database for the model calibration. The decision of choosing the three air temperatures is made considering the coverage of profound responses subject to a wide spectrum of moisture content. As a result, the calibrated parameters under such circumstance are achieved with trade-off to be able to predict close results as compared to the various experimental conditions. Note that only the dataset starting from the drying stage is used for model calibration as the drying stage is the utmost important process for the fluid bed dryer. The parameter estimation is carried out through the algorithm of MAXLHD in gPROMS. Table 6 summarizes the selected input parameters with initial value and calibrated values. The model calibration for FBD is carried out in the constant L/S ratio 0.25 whilst the calibrated parameters in TSG are directly from Table 5.

The fitted results are shown in Fig. 9 using the calibrated parameters in Table 6. In addition, the validated result under the air temperature 50 °C is shown in Fig. 9. As can be seen, the fitted results under the air temperature 40 °C, 60 °C and 70 °C give rise to relatively good agreement with the experimental results. Fig. 9 shows that the fully predictive validated result in air temperature 50 °C with the calibrated parameters shows very good closeness with the moisture content measured from NIR. It should be noted that the loading stage is not used for model validation due to the filling and drying of wet granules in the experiments. However, the drying curve from the flowsheet model is only seen to increase without fluctuation because only filling of wet granules is set up in gPROMS FBD model.

5.4. Cqas prediction based on validated process model

5.4.1. Global system analysis

Global System Analysis (GSA) provides a means to perform uncertainty analysis with Monte Carlo methods on the defined model for TSG and FBD. The GSA method assesses the uncertainty of the input variables imposed on the outcomes as responses. It should be noteworthy that prior knowledge of the input parameters in the defined model is critical to properly specify the variation regime for the input variables. Fig. 10 depicts the schematic of GSA in exploring the design space of CQAs based on the model inputs such as CPPs and Environmental inputs. x_1 and x_2 denote the single variable from the CPPs and environmental inputs. y_1 and y_2 denote the system output with x_1 and x_2 assigned to the system. The system generally represents a series of processes described by mixed differential and algebraic equations. In this study, the system is specific to the flowsheet modelling of integrated twin screw granulator and fluid bed dryer. The 'blue dot' x 'green square' denotes the combined action of a wide range of CPPs inputs (blue) and environmental inputs (green) which generates a range of system response, i.e. CQAs. The superiority of GSA is to overcome the limitation of local sensitivity analysis where the effect of input factors is studied around a reference point within a small space of variation. On the contrary, the GSA is able to compute the global sensitivity indices in an entire input regime and provide the crucial responses of the CQAs due to the variation of CPPs. Note the term L in the schematic denotes the local system analysis as compared to global system analysis.

The GSA performed in gPROMS includes two sample generation method, i.e. Quasi-random (Sobol) sampling and pseudo-random sampling. The global system analysis of the digital flowsheet of integrated TSG and FBD is based on uncertainty analysis of the Monte Carlo

Table 6

Selected input parameters in model validation of FBD.

Parameters for estimation	Initial value	Optimized value
Relative humidity in vapour (%)	1.0	0.1
Critical moisture content (kg/kg)	1.0	1.013
Sherwood number	0.4	0.368

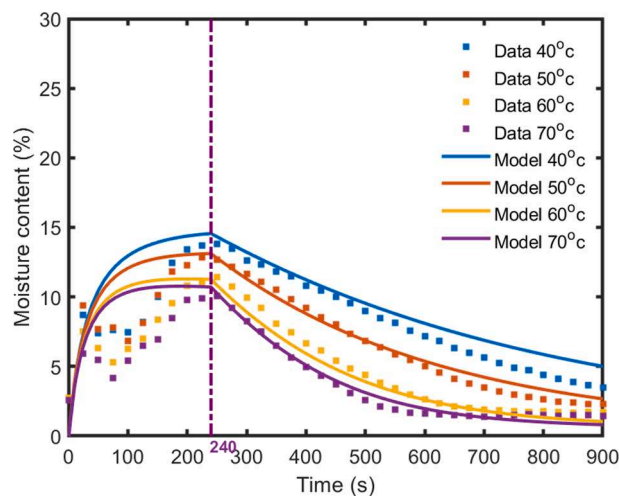


Fig. 9. Moisture content model calibration under air temperature 40 °C, 60 °C, 70 °C and model validation under air temperature 50 °C in fluid bed dryer.

method. More details about the uncertainty analysis, the sampling methods and procedures of carrying out GSA can be found elsewhere (Reis Sardinha, 2016).

5.4.2. Critical Quality attributes prediction based on model validation

The L/S ratio in TSG is first identified as the input factor in CPPs and its influence on the response of CQAs in TSG i.e. granule size distribution is carried out by means of GSA. The GSA of granule size distribution subject to the L/S ratios is plotted in Fig. 11. The liquid flow rate is varied as 1.0 to 4.0 kg/h, giving rise to the L/S ratio from 0.1 to 0.4 based on the constant solid feed rate 10 kg/h, compared to the experimental boundary of 0.15 and 0.35. 11 sampling points are assigned in the probability distribution and the response is the mass fraction of sieve classes identical to the setup in the experimental measurement. As the layering rate is interlinked with the L/S ratio in a linear way, the layering rate is also varied from 69.5 to 884 $\mu\text{m/s}$ in the GSA whilst the other parameters remain unchanged as the same value in the model validation. It can be clearly observed with increasing granules and decreasing fine powders when the L/S ratios is increased. The d_{50} of the granule size distribution based on sieve is summarized in Table 7, indicating a growth of d_{50} with increased L/S ratio.

The input factor selected for the FBD is the air temperature with the boundary values defined as 20 °C and 80 °C. Similarly, 7 points are assigned with incremental values of 10 as interval. The GSA of air temperature with its influence on the moisture content is shown in Fig. 12. It indicates a dramatic reduction of moisture content at the end of drying time 900 s when the air temperature is increased from 20 °C to 60 °C. Then the moisture content is gradually decreased with further increase until 80 °C.

An important feature of GSA is to explore the synergic effect of several CPPs on the response of CQAs. Hence, the combined effect of L/S ratios and air temperature is demonstrated as an example to explore the design space of final moisture content as the targeted CQA. The heat map of multivariate factors, i.e. L/S ratio and inlet air temperature is plotted in Fig. 13 via GSA. The experimental zone includes five data points of L/S ratios from 0.15 to 0.35 in TSG, which is used for model validation of granule size distribution. Whilst the experimental zone provides four data points subject to air temperature 40 °C, 50 °C, 60 °C, and 70 °C, the GSA of synergic effect of L/S ratio and air temperature clearly demonstrates a much wider spectrum of response for the final moisture content. It is found that increasing the L/S ratio to 0.4 and decreasing the air temperature to 20 °C results in the highest moisture content 18.43 %. Oppositely, the lowest moisture content arrives at 0.39 % at the lowest L/S ratio 0.1 and air temperature 80 °C. The moisture

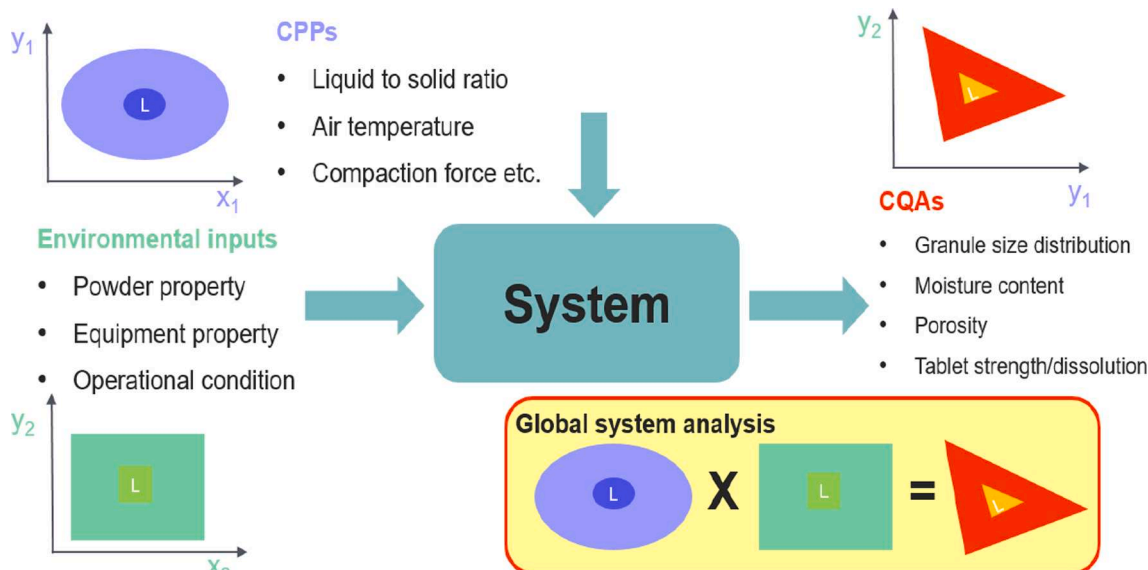


Fig. 10. Schematic of Global System Analysis considering the input and output categories.

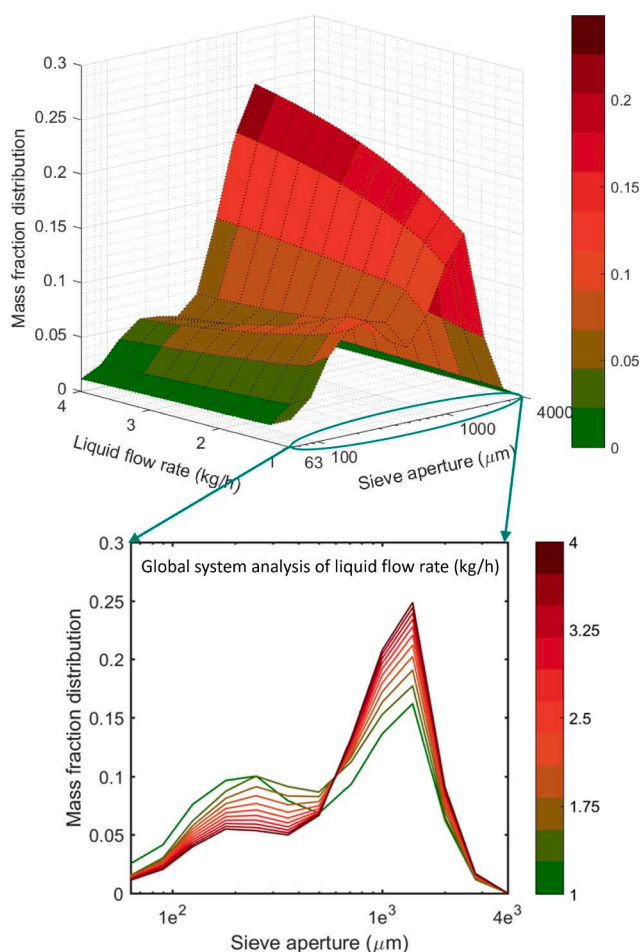


Fig. 11. Global system analysis of liquid flow rate on the granule size distribution.

content between 0.39 % and 18.43 % can be achieved according to the heat map, which provides a look-up table as the reference value and holds great promise in substantially reducing the amount of experiments in the current manufacturing activities.

Table 7
d₅₀ from granule size distribution based on Global system analysis.

Flow rate (kg/h)	L/S ratio	d ₅₀ (μm)
1.0	0.10	498.77
1.3	0.13	629.52
1.6	0.16	697.96
1.9	0.19	753.12
2.2	0.22	796.52
2.5	0.25	831.62
2.8	0.28	860.03
3.1	0.31	883.24
3.4	0.34	902.71
3.7	0.37	919.17
4.0	0.40	933.38

6. Conclusions

This paper presents a model-based process modelling of integrated twin screw granulator and fluid bed dryer, which are the key unit operations in the continuous manufacturing processes. As motivated by the approach of Model Driven Design (MDD), the model definition for TSG and FBD is first proposed, considering the mechanistically sound population, mass, energy equations. The best available models from either our previous work or the literature for the integrated TSG and FBD processes not only provide the mechanistic understanding of process dynamics but also pave a way for the success of model calibration and validation.

The experimental protocol is proposed in the continuous powder processing plant DiPP to provide the dataset required for the model calibration and validation. The criterion for experimental design in this work is to perform the least possible amount of experiments by identifying the most influential CPPs. As a result, the L/S ratio and air temperature are selected in TSG and FBD and their influence on the CQAs, i. e. granule size distribution and moisture content are inspected respectively.

A science-based digital-twin of the integrated TSG and FBD process was established in the advanced process modelling platform gPROMS. The predicted results in the model validation are shown to produce generally good agreement with the experimental data, with regard to the granule size distribution in TSG and moisture content in FBD. Despite only two CPPs, i.e. L/S ratio and air temperature used in the experimental design, the global system analysis (GSA) provides significant

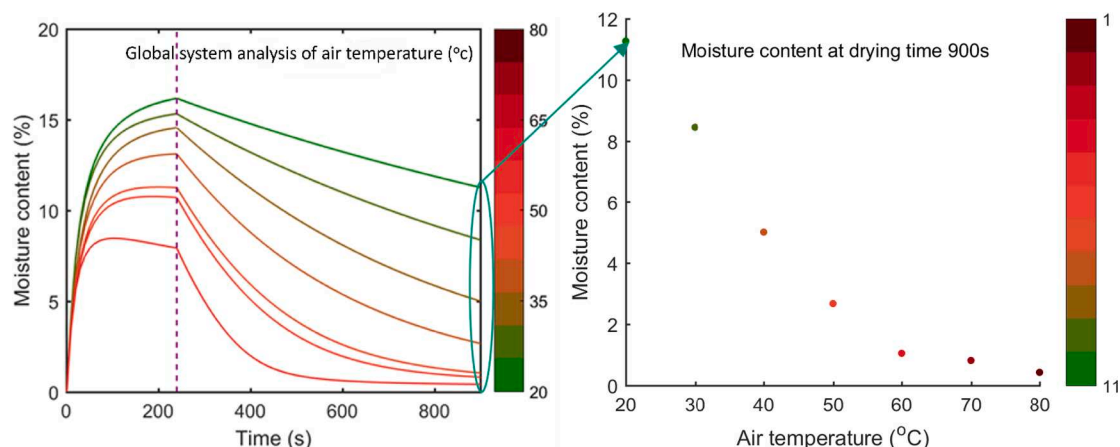


Fig. 12. Global system analysis of air temperature on the moisture content at 900 s.

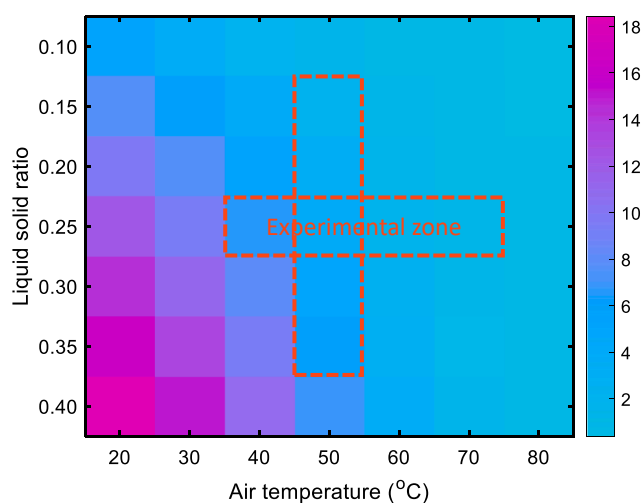


Fig. 13. Heat map of the effect of multiple variates, i.e. L/S ratio and air temperature on the final moisture content (%) via GSA.

insights on the exploration of design space with the confidence built from model validation. Most importantly, the GSA provides key scientific insights in establishing the relationship between CPPs and CQAs, which is currently lacking in the literature. The MDD approach for the integrated TSG and FBD provides proactive guidance and key insights in regulating the continuous manufacturing processes.

Appendix

Nucleation

The first rate process kernel occurring in the twin screw granulation is nucleation and the nucleation model is referred from the work of (Barrasso and Ramachandran, 2015). It gives.

$$B_{nuc} = \frac{L_{in,powder}(x,t)}{V_{droplet}} \quad (20)$$

where B_{nuc} is the nucleation rate; $L_{in,powder}(x,t)$ is the rate of liquid addition to the fine powder; $V_{droplet}$ is the volume of a single liquid droplet, which is assumed to be spherical.

Breakage

The breakage kernel in the twin screw granulation is composed of two functions, i.e. the selection function S_M and the breakage function b_M . As stated in the model assumptions, the breakage mechanisms are distinguished by two breakage modes dependent on the screw elements. The

CRediT authorship contribution statement

Li Ge Wang: Methodology, Software. **Chalak Omar:** Data curation, Writing – original draft. **James Litster:** Conceptualization, Investigation, Supervision. **David Slade:** Supervision. **Jianfeng Li:** Software. **Agba Salman:** Supervision. **Stefan Bellinghausen:** Software. **Dana Barrasso:** Software. **Niall Mitchell:** Supervision.

Declaration of Competing Interest

The authors declare that they have no known competing financial interests or personal relationships that could have appeared to influence the work reported in this paper.

Data availability

Data will be made available on request.

Acknowledgement

The writers gratefully acknowledge the financial support from Innovate UK for the Knowledge Transfer Partnership Grant No. 158229 between The University of Sheffield and Siemens Process Systems Engineering. We would like to thank Prof. Costas Pantelides, Dr Sean Birmingham from Siemens Process Systems Engineering and Dr. Matthew Hogan from Knowledge Transfer Network for their advice, feedback and support.

mechanistic breakage kernel proposed in this work is based on our previous work (Wang et al., 2020). The screw-dependent selection functions to describe the breakage probability of granules are given as follows:

Screw elements	Selection function
Conveying elements	$P_b = \begin{cases} 1 & x \geq x_{uc} \\ a_{SF,CE} * \exp\left(-\frac{DYS}{b_{SF,CE}} * \frac{1}{PFN}\right) * (x/x_{lc})^{c_{SF,CE}} & x_{lc} < x < x_{uc} \\ 0 & x \leq x_{lc} \end{cases} \quad (21)$
Kneading elements	$P_b = \begin{cases} 1 & x \geq x_{uc} \\ 1 - a_{SF,KE} * \exp\left(-PFN * \frac{b_{SF,KE}}{DYS} * \left(\frac{x}{x_{lc}}\right)^{c_{SF,KE}}\right) & x_{lc} < x < x_{uc} \\ 0 & x \leq x_{lc} \end{cases} \quad (22)$

where P_b is the breakage probability; DYS and PFN are the Dynamic yield strength and powder feed number, respectively; a , b , and c are fitting parameters; The subscripts of SF, CE and KE denote selection function, conveying element and kneading element. x_{lc} and x_{uc} are lower and upper critical breakage size of granules.

The screw-dependent breakage functions to describe the breakage granule size distribution are given as follows:

Screw elements	Breakage function
Conveying elements	$B_{CE} = \nu B_{x1} + (1 - \nu) B_{x2} \quad (23)$
Kneading elements	$B_{KE} = 1 - \exp\left(-a_{BF,KE} * \left(\frac{x}{x_{lc}}\right)^{b_{BF,KE}}\right) \quad (24)$

where B_{CE} and B_{KE} are the cumulative size distribution CEs and KEs. B_{x1} and B_{x2} are the modified Weibull distribution, identical to the form in Eq. (7). a is the scale parameter and b is the shape parameter in the Weibull function. The subscripts of BF and KE denote breakage function and kneading element.

Layering

Layering plays a role in the granule growth as fine powders adhere to the wet surface of agglomerate. This process is strongly dependant on the friction of fine powders and the moisture content of granules. The layering rate is given by (Cameron et al., 2005).

$$\frac{dn}{dt} = G_m \frac{M_{powder}}{k_l M_{granule} + M_{powder}} \exp[-a(x_w - x_{wc})^2] \quad (25)$$

where G_m is the maximum growth rate, M_{powder} and $M_{granule}$ are the mass of fine powder below the lower bound of the particle classes and the mass of granule respectively. x_w is the moisture content whilst x_{wc} is the critical moisture content; k_l and a are fitting parameters. As shown in Eq. (8), the linear growth rate due to layering is not dependent on granule size. Small granules experience a more dramatic increase in size than large granules because of their high surface area-to-volume ratios. Furthermore, breakage can facilitate layering by increasing the overall surface area of the granulate phase.

Consolidation

The granule consolidation rate is given (Iveson et al., 1996):

$$\frac{d\varepsilon}{dt} = -k_c (\varepsilon - \varepsilon_{min}) \quad (26)$$

where ε is the granule porosity at time t ; k_c is the granule compaction rate; ε_{min} is the minimum porosity for consolidation to occur.

The consolidation rate is reported to be dependent on impact forces due to particle collisions with each other or the TSG equipment (Barrasso and Ramachandran, 2015). As a result, the consolidation results in less porous granules with increased density.

References

Barrasso, D., El, A., Litster, J.D., Ramachandran, R., 2015. Multi-dimensional population balance model development and validation for a twin screw granulation process. Powder Technol. 270, 612–621. <https://doi.org/10.1016/j.powtec.2014.06.035>.

Barrasso, D., Ramachandran, R., 2016. Qualitative Assessment of a Multi-Scale, Compartmental PBM-DEM Model of a Continuous Twin-Screw Wet Granulation Process. J. Pharm. Innov. 11, 231–249. <https://doi.org/10.1007/s12247-015-9240-7>.

Barrasso, D., Ramachandran, R., 2015. Multi-scale modeling of granulation processes: Bi-directional coupling of PBM with DEM via collision frequencies. Chem. Eng. Res. Des. 93, 304–317. <https://doi.org/10.1016/j.cherd.2014.04.016>.

Boukouvala, F., Niotis, V., Ramachandran, R., Muzzio, F.J., Ierapetritou, M.G., 2012. An integrated approach for dynamic flowsheet modeling and sensitivity analysis of a continuous tablet manufacturing process. Comput. Chem. Eng. 42, 30–47. <https://doi.org/10.1016/j.compchemeng.2012.02.015>.

Burgschweiger, J., Tsotsas, E., 2002. Experimental investigation and modelling of continuous fluidized bed drying under steady-state and dynamic conditions. Chem. Eng. Sci. 57, 5021–5038. [https://doi.org/10.1016/S0009-2509\(02\)00424-4](https://doi.org/10.1016/S0009-2509(02)00424-4).

- Cameron, I.T., Wang, F.Y., Immanuel, C.D., Stepanek, F., 2005. Process systems modelling and applications in granulation: A review. *Chem. Eng. Sci.* 60, 3723–3750. <https://doi.org/10.1016/j.ces.2005.02.004>.
- De Leersnyder, F., Vanhoorne, V., Bekaert, H., Vercruyse, J., Ghijs, M., Bostijn, N., Verstraeten, M., Cappuyns, P., Van Assche, I., Vander Heyden, Y., Ziemons, E., Remon, J.P., Nopens, I., Vervaet, C., De Beer, T., 2018. Breakage and drying behaviour of granules in a continuous fluid bed dryer: Influence of process parameters and wet granule transfer. *Eur. J. Pharm. Sci.* 115, 223–232. <https://doi.org/10.1016/j.ejps.2018.01.037>.
- Dhenge, R.M., Fyles, R.S., Cartwright, J.J., Doughty, D.G., Hounslow, M.J., Salman, A.D., 2010. Twin screw wet granulation: Granule properties. *Chem. Eng. J.* 164, 322–329. <https://doi.org/10.1016/j.cej.2010.05.023>.
- El Hagrasy, A.S., Hennenkamp, J.R., Burke, M.D., Cartwright, J.J., Litster, J.D., 2013. Twin screw wet granulation: Influence of formulation parameters on granule properties and growth behavior. *Powder Technol.* 238, 108–115. <https://doi.org/10.1016/j.powtec.2012.04.035>.
- El Hagrasy, A.S., Litster, J.D., 2013. Granulation rate processes in the kneading elements of a twin screw granulator. *AIChE J.* 59, 4100–4115. <https://doi.org/10.1002/aic.14180>.
- Fonteyne, M., Arruabarrena, J., de Beer, J., Hellings, M., Van Den Kerkhof, T., Burggraef, A., Vervaet, C., Remon, J.P., De Beer, T., 2014. NIR spectroscopic method for the in-line moisture assessment during drying in a six-segmented fluid bed dryer of a continuous tablet production line: Validation of quantifying abilities and uncertainty assessment. *J. Pharm. Biomed. Anal.* 100, 21–27. <https://doi.org/10.1016/j.jpba.2014.07.012>.
- Fonteyne, M., Vercruyse, J., Díaz, D.C., Gildemyn, D., Vervaet, C., Remon, J.P., Beer, T. D., 2013. Real-time assessment of critical quality attributes of a continuous granulation process. *Pharm. Dev. Technol.* 18, 85–97. <https://doi.org/10.3109/10837450.2011.627869>.
- Fries, L., Dosta, M., Antonyuk, S., Heinrich, S., Palzer, S., 2011. Moisture distribution in fluidized beds with liquid injection. *Chem. Eng. Technol.* 34, 1076–1084. <https://doi.org/10.1002/ceat.201100132>.
- García-Muñoz, S., Butterbaugh, A., Leavesley, I., Manley, L.F., Slade, D., Birmingham, S., 2018. A flowsheet model for the development of a continuous process for pharmaceutical tablets: An industrial perspective. *AIChE J.* 64, 511–525. <https://doi.org/10.1002/aic.15967>.
- gPROMS Formulated Products Release 1.6, 2020.
- Iveson, S.M., Litster, J.D., Ennis, B.J., 1996. Fundamental studies of granule consolidation part 1: Effects of binder content and binder viscosity. *Powder Technol.* 88, 15–20. [https://doi.org/10.1016/0032-5910\(96\)03096-3](https://doi.org/10.1016/0032-5910(96)03096-3).
- Kumar, A., Vercruyse, J., Mortier, S.T.F.C., Vervaet, C., Remon, J.P., Gernaey, K.V., De Beer, T., Nopens, I., 2016. Model-based analysis of a twin-screw wet granulation system for continuous solid dosage manufacturing. *Comput. Chem. Eng.* 89, 62–70. <https://doi.org/10.1016/j.compchemeng.2016.03.007>.
- Lee, S.L., O'Connor, T.F., Yang, X., Cruz, C.N., Chatterjee, S., Madurawe, R.D., Moore, C. M.V., Yu, L.X., Woodcock, J., 2015. Modernizing Pharmaceutical Manufacturing: from Batch to Continuous Production. *J. Pharm. Innov.* 10, 191–199. <https://doi.org/10.1007/s12247-015-9215-8>.
- Liu, H., Galbraith, S.C., Park, S.-Y., Cha, B., Huang, Z., Meyer, R.F., Flamm, M.H., O'Connor, T., Lee, S., Yoon, S., 2018. Development of a three-compartmental population balance model for a continuous twin screw wet granulation process. *Pharm. Dev. Technol.* 1–39. <https://doi.org/10.1080/10837450.2018.1427106>.
- Liu, H., Ricart, B., Stanton, C., Smith-Goettler, B., Verdi, L., O'Connor, T., Lee, S., Yoon, S., 2019. Design space determination and process optimization in at-scale continuous twin screw wet granulation. *Comput. Chem. Eng.* 125, 271–286. <https://doi.org/10.1016/j.compchemeng.2019.03.026>.
- Matsunami, K., Nagato, T., Hasegawa, K., Sugiyama, H., 2020. Determining key parameters of continuous wet granulation for tablet quality and productivity: A case in ethenzamide. *Int. J. Pharm.* 579, 119160. <https://doi.org/10.1016/j.ijpharm.2020.119160>.
- McGuire, A.D., Mosbach, S., Reynolds, G.K., Patterson, R.I.A., Bringley, E., Eaves, N., Dreyer, J.A.H., Kraft, M., 2019. Analysing the effect of screw configuration using a stochastic twin-screw granulation model. *Chem. Eng. Sci.* 203, 358–379. <https://doi.org/10.1016/j.ces.2019.03.078>.
- Meng, W., Rao, K.S., Snee, R.D., Ramachandran, R., Muzzio, F.J., 2019. A comprehensive analysis and optimization of continuous twin-screw granulation processes via sequential experimentation strategy. *Int. J. Pharm.* 556, 349–362. <https://doi.org/10.1016/j.ijpharm.2018.12.009>.
- Metta, N., Ghijs, M., Schäfer, E., Kumar, A., Cappuyns, P., Van Assche, I., Singh, R., Ramachandran, R., De Beer, T., Ierapetritou, M., Nopens, I., 2019. Dynamic flowsheet model development and sensitivity analysis of a continuous pharmaceutical tablet manufacturing process using the wet granulation route. *Processes* 7, 1–35. <https://doi.org/10.3390/pr7040234>.
- Monaco, D., Omar, C., Reynolds, G.K., Tajarobi, P., Litster, J.D., Salman, A.D., 2021. Drying in a continuous wet granulation line: Investigation of different end of drying control methods. *Powder Technol.* 392, 157–166. <https://doi.org/10.1016/j.powtec.2021.07.004>.
- Mortier, S.T.F.C., De Beer, T., Gernaey, K.V., Remon, J.P., Vervaet, C., Nopens, I., 2011. Mechanistic modelling of fluidized bed drying processes of wet porous granules: A review. *Eur. J. Pharm. Biopharm.* 79, 205–225. <https://doi.org/10.1016/j.ejpb.2011.05.013>.
- Pauli, V., Elbaz, F., Kleinbudde, P., Krumme, M., 2018. Methodology for a Variable Rate Control Strategy Development in Continuous Manufacturing Applied to Twin-screw Wet-Granulation and Continuous Fluid-bed Drying. *J. Pharm. Innov.* 13, 247–260. <https://doi.org/10.1007/s12247-018-9320-6>.
- Peglow, M., Kumar, J., Heinrich, S., Warnecke, G., Tsotsas, E., Mörl, L., Wolf, B., 2007. Drying in a continuous wet granulation model for simultaneous agglomeration and drying in fluidized beds. *Chem. Eng. Sci.* 62, 513–532. <https://doi.org/10.1016/j.ces.2006.09.042>.
- Poós, T., Szabó, V., 2021. Modeling of heat and mass transfer in fluidized bed dryers using the volumetric heat transfer coefficient. Part 1: Equations describing the simultaneous heat and mass transfer. *Dry. Technol.* 1–10. <https://doi.org/10.1080/07373937.2021.1938112>.
- Reis Sardinha, H., 2016. Mechanistic Modelling of Product Degradation.
- Sayin, R., Martinez-Marcos, L., Osorio, J.G., Cruise, P., Jones, I., Halbert, G.W., Lamprou, D.A., Litster, J.D., 2015. Investigation of an 11 mm diameter twin screw granulator: Screw element performance and in-line monitoring via image analysis. *Int. J. Pharm.* 496, 24–32. <https://doi.org/10.1016/j.ijpharm.2015.09.024>.
- Shirazian, S., Ismail, H.Y., Singh, M., Shaikh, R., Croker, D.M., Walker, G.M., 2019. Multi-dimensional population balance modelling of pharmaceutical formulations for continuous twin-screw wet granulation: Determination of liquid distribution. *Int. J. Pharm.* 566, 352–360. <https://doi.org/10.1016/j.ijpharm.2019.06.001>.
- Van Hauwermeiren, D., Verstraeten, M., Doshi, P., am Ende, M.T., Turnbull, N., Lee, K., De Beer, T., Nopens, I., 2019. On the modelling of granule size distributions in twin-screw wet granulation: Calibration of a novel compartmental population balance model. *Powder Technol.* 341, 116–125. <https://doi.org/10.1016/j.powtec.2018.05.025>.
- Wang, L.G., Morrissey, J.P., Barrasso, D., Slade, D., Clifford, S., Reynolds, G., Ooi, J.Y., Litster, J.D., 2021a. Model Driven Design for Twin Screw Granulation using Mechanistic-based Population Balance Model. *Int. J. Pharm.* 607, 120939. <https://doi.org/10.1016/j.ijpharm.2021.120939>.
- Wang, L.G., Omar, C., Litster, J.D., Li, J., Mitchell, N., Bellinghausen, S., Barrasso, D., Salman, A., Slade, D., 2021b. Tableting model assessment of porosity and tensile strength using a continuous wet granulation route. *Int. J. Pharm.* 607, 120934. <https://doi.org/10.1016/j.ijpharm.2021.120934>.
- Wang, L.G., Pradhan, S.U., Wassgren, C., Barrasso, D., Slade, D., Litster, J.D., 2020. A breakage kernel for use in population balance modelling of twin screw granulation. *Powder Technol.* 363, 525–540. <https://doi.org/10.1016/j.powtec.2020.01.024>.
- Yu, L.X., Amidon, G., Khan, M.A., Hoag, S.W., Polli, J., Raju, G.K., Woodcock, J., 2014. Understanding pharmaceutical quality by design. *AAAPS J.* 16, 771–783. <https://doi.org/10.1208/s12248-014-9598->